CrossMark

Energy analysis for guiding the design of well systems of deep Enhanced Geothermal Systems

Mengying Li, Noam Lior[*]

University of Pennsylvania, Department of Mechanical Engineering and Applied Mechanics, Philadelphia, PA 19104-6315, USA

ABSTRACT

The focal objective of this work is to calculate the energy consumption for constructing the EGS (Enhanced Geothermal Systems) wells, to examine the energy (heat and power) performance of such well systems, and to propose and evaluate several ways for improving that performance. A model was developed to compute the pressure and temperature fields of the geofluid flowing in the production and injection wells to be able to calculate the flow pumping energy consumption, and the heat gain/loss during its flow in/out of the enhanced reservoir, for wells up to 10 km deep. The total well construction energy consumption was calculated to be 19.40 TJ/(km of well) for the considered well configurations, and increases approximately linearly with the flow cross section area of the well. Several ways to improve the energy performance of the wells, by increasing the heat output of the production wells and decreasing the required power for pumping the geofluid were evaluated: (1) increasing the number of injection/production wells to reduce the pressure drop in each, (2) increasing the flow cross section of the injection/projection well, and (3) adding thermal insulation to the circumference of the production wells (to reduce the geofluid heat loss to the rock). Most of these methods were found to indeed increase the power output of the geothermal system but have increased the construction energy requirement somewhat more. More energy efficient drilling methods and materials of lower embodied energy can lead to a higher EROI (energy return on investment). The EROI of the recommended EGS well system designs ranged from 33.8 to 286.2.

© 2015 Elsevier Ltd. All rights reserved.

1. Introduction

Geothermal energy is abundant, practically renewable, and has a long-term potential estimated to be more than 200,000-fold of current world energy demand [1]. In the continental United States, over 99% of the geothermal heat within depths of about 10 km is available in HDR (hot dry rock) where little natural fluid exists and the rock has low permeability [1,2]. One characteristic of an HDR resource is the geothermal gradient ($G\,°C/km$), which quantifies the temperature increase with resource depth. To extract the geothermal heat, a large volume of the hot rock (reservoir) must be fractured in the high geothermal gradient region (Fig. 1). The fractures are created by means of hydro-fracturing and etc. [1] to allow liquid flow through the hot rock. Injection and production wells are drilled to connect the fractures to allow liquid circulation between the reservoir and the surface structures. Cold fluid

("geofluid", usually water) is injected into this reservoir to be heated and brought back to the surface for direct use or for generating electricity in a power plant. The injection wells (IW-s), production wells (PW-s), fractured reservoir and surface power plant constitute a typical EGS (Enhanced Geothermal System) where IW-s and PW-s are essential components of an EGS system, which connect the engineered reservoir with the surface power plant.

To bring as much thermal energy to the surface while incurring least energy consumption, the design goals for IW-s and PW-s should be to minimize:

(1) The energy consumption for constructing the wells.
(2) The heat losses from the geofluid to surrounding rock during its flow through the PW-s.
(3) The pumping energy consumption for driving the geofluid flow through these wells.

The focal objective of this work is therefore to calculate the energy consumption of constructing the EGS wells (Section 2), and

* Corresponding author. 220 S. 33rd Street, 212 Towne Building, Philadelphia, PA 19104, USA. Tel.: +1 215 898 4803.
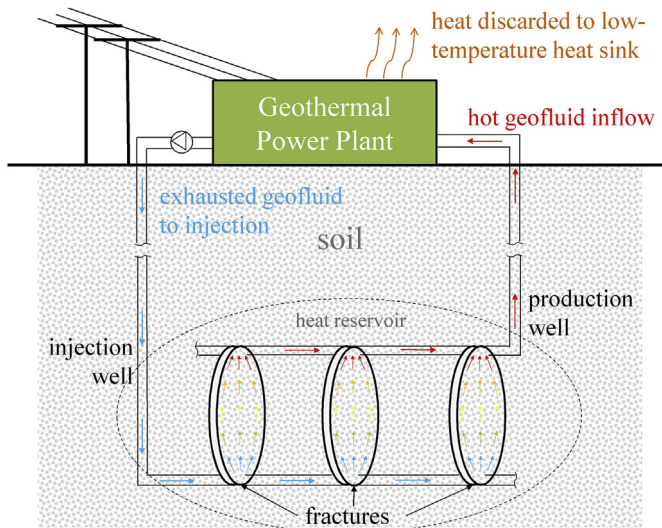E-mail address: lior@seas.upenn.edu (N. Lior).

Fig. 1. Schematic diagram of an EGS system [1,3].

to model the pressure and temperature fields of the geofluid flowing in the wells to be able to calculate the flow pumping energy consumption, and the heat gain/loss during its flow in/out of the engineered reservoir (Section 3). Since deeper reservoirs typically contain more heat and that at higher temperature, they require longer and deeper wells that negate some of the benefit because they require more energy for their construction and also incur higher heat and pressure losses. It thus clearly poses a design optimization problem focused on maximizing overall energy performance, addressed here by varying the reservoir depth, number of wells, well flow cross sections and the best energy performance design are proposed (Section 4).

While costs are of paramount importance, this study was focused on the energy analysis because (1) energy perspective analyses are lacking in the published literature while cost analyses are widely available [1,4,5]. (2) Knowledge of energy quantities can be translated relatively easily to costs if the price of energy, which fluctuates wildly, is known.

Nine cases were calculated: 3 depths each at 3 geothermal gradients, as shown in Table 1, assuming in all that the ground surface temperature is $T_s = 15\ °C$ [6]. The average PW bottom temperature $T_{b,pw}$ (assumed to be equal to the reservoir temperature) is:

$$T_{b,pw} = 15 + Z \cdot G, \tag{1}$$

where Z is the well depth (km) and G is the geothermal gradient (°C/km).

When the geofluid is injected into the EGS subsurface system (wells and reservoirs), it is preferred to keep it in the liquid phase throughout the subsequent heating and recovery process, rather than allow it to flash or otherwise evaporate, as explained in Refs. [2] and [7]. To accomplish this, the pressure in the subsurface system must be maintained high enough to keep the hot liquid below its boiling point.

The contribution of this work is to examine quantitatively the energy input and output for typical EGS wells in an EGS system (the analysis of the power generation plant and engineered reservoirs can be found in Refs. [3] and [8]), and examine their sensitivity to the number of IW/PW, flow cross section of IW/PW and adding insulation to PW-s, for ultimately proposing highest net energy output well system design. Here the energy input is the energy consumption for constructing the wells. The energy output is the electricity generated by the EGS power plant minus the geofluid circulating pumping energy. The temperature and pressure changes of the geofluid flowing through the wells are calculated by a finite difference method.

The detailed contributions of this work are:

(1) Our calculations extend to well depths of 10 km.
(2) A simplified mathematical model was developed and used to compute the EGS well construction energy consumption.
(3) A model for flow and heat transfer in EGS wells was developed to include both subcritical and supercritical geofluid and density changes in wells.
(4) Methods that improve the performance of IW/PW were examined. They include the possibility to add more IW/PW, to enlarge the flow cross section areas of IW/PW and to add thermal insulation to the PW-s.

2. Energy consumption for constructing EGS wells

The drilling process of EGS wells is in many ways similar to that used for the gas and oil. After exploration to determine the location, the drilling rig is set in place. The drilling rig creates a hold to the ground and provides the torque to rotate the drill bits and power to circulate drilling mud (fluid to lubricate and cool the bits and remove the cuttings while drilling). The rig also provides monitoring equipment along the well to do measurements and diagnosis needed for the well drilling process.

In the traditional drilling method, rock in the drill's path is broken into small pieces under the high pressure applied by the drill bits. A hole of desired depth is created typically in a few months. There are also proposals for novel drilling methods like jet drilling and thermal drilling as introduced in Refs. [9] and [10].

After creating the hole, it needs to be cased and cemented to complete the well (Fig. 2). Casing is to install permanent hardware (usually metal tubes) inside the borehole to maintain its integrity and isolate it from its surrounding environment. After casing, the gaps between casings and the borehole are filled with cement [11]. The geofluid in EGS applications flows inside the inner diameter of the casing.

The well system of deep EGS consists of at least one IW and one PW. More than one PW per IW is common. For example, there are doublets, one IW for one PW; triplets, two PW-s for each IW; quartet, three PW-s with a single IW and five-spots, and so on [1].

After reaching the desired depth, the wells must typically be deviated to a horizontal section into the reservoir region (Fig. 1) to eventually stimulate (fracture) it. The deviated well arrangement offers a larger drilling window along the created horizontal part, and could create nearly parallel vertical fracture [1,11]. The casing in

Table 1
Average PW bottom temperatures $T_{b,pw}$ for the depths and geothermal gradients considered in this work.

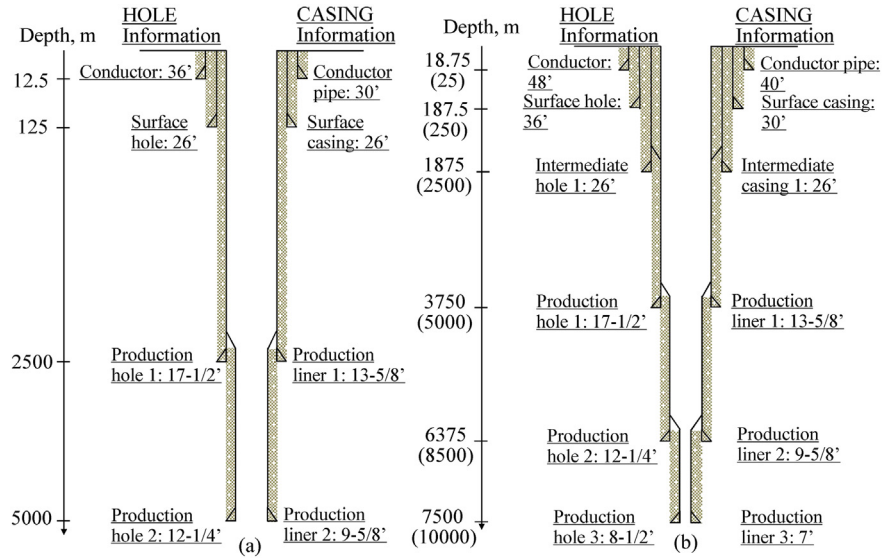| Geothermal gradient G, °C/km	40			60			80		
Well depth Z, km	5	7.5	10	5	7.5	10	5	7.5	10
Average PW bottom temperature $T_{b,pw}$, °C	215	315	415	315	465	615	415	615	815

Fig. 2. Configurations of (a) 5 km wells and (b) 7.5 and 10 km wells [1,11]. In (b), the numbers in parenthesis represents 10 km wells.

the deviated part of the IW in the reservoir region is perforated to allow hydro-fracturing [1]. As discussed in Ref. [3], the length of the deviated part is a product of the chosen number of fractures in the reservoir and the distance between them. That inter-fracture distance was found in Ref. [3] to be 120 m to maintain the heat extraction decay from the rock within 10% during 40 years of operation and to make the thermal interference between adjacent fractures negligible.

The length of the deviated part, shown in Table 2 is calculated based on the recommended number of fractures from Ref. [3] (under certain assumptions). Since the number of fractures is highly dependent on how fast the heat extraction from the reservoir decay one can tolerate that beyond the scope of this work, in the following analysis, we only consider the vertical part of the wells.

In this study, the borehole is considered to be drilled using PDC (polycrystalline diamond compact) and roller cone hybrid bits [12] in a traditional drilling method. The energy for drilling EGS wells consists of three parts: the energy consumed to create the borehole and operating casing and cementing (drilling operation), the embodied energy of well casings and cement and other miscellaneous such as the embodied energy of the drilling mud.

2.1. Well configurations

Studies in Ref. [4] identified that the need for an increasing number of casing strings or liners with depth is a reason for the significant increase of drilling costs with depth. A liner is a special casing string that does not extend to the top of the wellbore, but instead is anchored or suspended from inside the bottom of the previous casing string [13]. Ref. [1] provides the recommended number of casing strings or liners of EGS wells for different depths, and the information is reproduced in Table 3. For wells over 6 km

deep, liners instead of casing strings can be used to reduce the casing cost [11].

We therefore chose 4 casing strings/liners for the 5 km well, and 6 casing strings/liners for the 7.5 km and 10 km wells, and assumed that wells with the same number of casing strings/liners have the same well configurations [1], as shown in Fig. 2 (b), and that the 7.5 km and 10 km wells have the same configurations.

PW-s are of same configuration design as corresponding IW-s of the same depth. The number of PW-s per IW depends on the temperature and pressure changes of the geofluid transporting in them (Section 4).

2.2. Energy consumption of the drilling operation

According to Ref. [11], making a 6 km well (including borehole creation and casings/cement operation) requires 8475 kg/day of diesel fuel. The specific chemical energy of the diesel fuel is 45.3 MJ/kg [14], thus the daily chemical energy consumption is $\dot{E}_{dr} = 0.384$ TJ/day. The energy is for rotating the drill bits and operating the drilling mud pump, as well as for installing the casings and cementing. For different types of soil and underground rock stresses, the rate of penetration (ROP, m/day) would differ, and so would the time required to drill wells of the same depth. For typical drilling conditions considered in Ref. [11], the ROP for different borehole diameters is listed in Table 4, which, incidentally, also shows that it is not directly proportional to the borehole diameter. The total drilling time is around 1.554 times of borehole creation time, which takes into consideration the additional time needed for installing the casings and for cementing [11].

The total energy consumption of the drilling operation can thus be calculated as:

Table 2
Length of the horizontal part of wells for the depths and geothermal gradient considered in this work.

Well depth Z, km	5			7.5			10		
Geothermal gradient G, °C/km	40	60	80	40	60	80	40	60	80
Recommended number of fractures [3]	30	23	19	10	8	7	5	4	4
Length of horizontal part of well, km	3.60	2.76	2.28	1.20	0.96	0.84	0.60	0.48	0.48

Table 3
Number of recommended casing strings or liners for EGS wells (from Ref. [1]).

Depth, km	1.5	2.5	3	4	5	5	6	6	7.5	10
No. of Casing Strings	4	4	4	4	4	5	5	6	6	6

Table 4
Energy consumption of borehole creation for 5 km, 7.5 km and 10 km wells.

Hole diameters D_{wb}, inch (Fig. 2)	ROP, m/day [11]	Drilling length L_{dr}, m (Fig. 2)		
Well depth, km		5	7.5	10
36″	33.5	0	168.75	225
26″	83.8	112.5	1687.5	2250
17-1/2″	83.8	2375	1875	2500
12-1/4″	62.5	2500	2625	3500
8-1/2″	45.7	0	1125	1500
Sum		4987.5	7481.25	9975
Energy consumed, TJ (Eq. (2))		42.9	70.3	93.7

$$E_{dr} = \frac{\dot{E}_{dr} L_{dr}}{\text{ROP}}. \tag{2}$$

where L_{dr} is the drilling distance (m).

The energy consumptions for borehole creation we calculated using Eq. (2) are listed in Table 4. Columns 1 and 3–5 of the table present the diameter and length of the considered well segments (Fig. 2) and column 2 presents the ROP values obtained from Ref. [11].

2.3. The embodied energy of well casings and cement

Typically, the well casings are made of stainless steels to resist corrosion from the geofluid, and the cementing material is Portland cement [15]. The specific embodied energy of stainless steel is $b_{cs} = 56.7$ MJ/kg and of Portland cement is $b_{cm} = 5.5$ MJ/kg [16]. The unit casing weights are found from the American Petroleum Institute casing dimensions chart [17] and reference [11], where casing thickness is dependent on its diameter.

The casing stainless steels embodied energy is thus:

$$B_{cs} = b_{cs} M_{cs} \tag{3}$$

where M_{cs} is the mass of casing (kg).

The embodied energy of the cement is,

$$B_{cm} = b_{cm} M_{cm} = b_{cm} \rho_{cm} \frac{\pi}{4} \left(D_{wb}^2 - D^2 \right) L_c, \tag{4}$$

where M_{cm} is the mass of cement (kg), ρ_{cm} is the density of cement (1522 kg/m^3 [18]), D_{wb} is the diameter of wellbore (m), D is the diameter of casing (m) and L_c is the length of casings/cement well segment (m).

Table 5 presents the embodied energy of casing and cement for 5 km, 7.5 km and 10 km wells. Column 3 presents the unit casing weight obtained from Refs. [11] and [17], columns 4–6 present the casings/cement length of well segments, columns 7–9 present the calculated casing mass, which equals to the length of the casing multiplied by the corresponding unit weight, columns 10–12 present the calculated cement mass, using Eq. (4). The embodied energy of casing and cements are also presented in Table 5.

The total energy consumption of well construction is:

$$E_{well} = E_{dr} + B_{cs} + B_{cm} + E_{other}. \tag{5}$$

where E_{other} (TJ) represents the embodied energy of drilling mud, the energy consumption of measurements and diagnosis during drilling and are obtained from Ref. [19].

2.4. Well construction analysis results and discussion

The construction energy consumptions for wells of depths 5, 7.5 and 10 km, calculated by using Eqs. (2)–(5) are shown in Fig. 3. The drilling energy consumption and casings' embodied energy compose over 93.1% of the total energy consumption while the cement embodied energy and the miscellaneous energy consists less than 6.9%. The associated embodied energy requirement was found to be about 43.0%–49.8% of the total energy requirement. The well construction energy increases nearly linearly with depth (Fig. 3). The specific energy consumption is $e_{well} = 19.4$ TJ/(km of well).

To validate our calculations, we compared our results with those in Ref. [19] and the comparisons are listed in Table 6, which show that they are within ±7%. It is noteworthy that our calculations are simpler, more detailed and easier to duplicate.

A dimensionless parameter A^* is defined to indicate the relative flow cross section area of a well compared to the wells in Fig. 2, where $A^* = 2$ indicates that the flow cross section area of the well is doubled (i.e. the diameter is enlarged $\sqrt{2}$ times) and $A^* = 3$ indicates that the flow cross section area of the well is tripled (the diameter is enlarged $\sqrt{3}$ times). For $A^* = 1$, the energy requirement to construct a well is presented in Fig. 3. For $A^* = 2$, the volume of rock that must be removed is doubled and the casing and cement material weight is doubled. So the energy consumed to construct a well is approximately doubled. In a similar way, for $A^* = 3$, the energy consumed to construct a well is approximately tripled.

To reduce the heat exchange between geofluid in the wells and surrounding rock, the cement can be replaced by a more thermal insulating material, such as ceramic insulation. For the magnesia

Table 5
Embodied energy of casing and cement for 5 km, 7.5 km and 10 km deep wells.

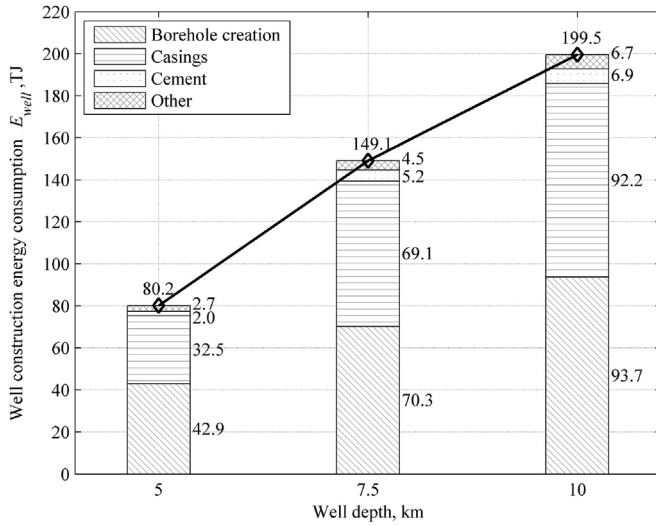| Column 1	2	3	4	5	6	7	8	9	10	11	12
Hole diameters D_{wb}, inch (Fig. 2)	Casing diameter D, inch (Fig. 2)	Unit casing weight, kg/m [11,17]	Casing length/Cementing length L_c, m (Fig. 2)			Casing mass M_{cs}, ton (Casing length × unit casing weight)			Cement mass M_{cm}, ton (Eq. (4))		
Well depth, km			5	7.5	10	5	7.5	10	5	7.5	10
36″	30″	460.73	0	187.5	250	0.0	55.7	74.2	0.0	57.2	76.3
26″	26″	251.17	125	1875	2500	24.7	371.1	494.8	26.6	398.9	531.9
17-1/2″	13-5/8″	131.08	2500	3750	5000	267.9	401.8	535.8	232.4	348.6	464.8
12-1/4″	9-5/8″	79.62	2500	2625	3500	281.3	295.3	393.8	110.7	116.2	154.9
8-1/2″	7″	47.62	0	1125	1500	0.0	95.6	127.5	0.0	20.2	26.9
Sum						573.9	1219.5	1626.0	369.7	941.1	1254.8
Embodied energy, TJ (Eqs. (3)–(4))						32.5	69.1	92.2	2.03	5.18	6.90

Fig. 3. Itemized and total (numbers on top of each bar) well construction energy consumption as a function of well depth.

considered here the thermal conductivity ($k_m = 0.07$ W/(m K) [20]) is 4.12-fold lower than that of Portland cement ($k_{cm} = 0.29$ W/(m K) [20]). The magnesia is much more expensive than cement, and its specific embodied energy is $b_m = 45$ MJ/kg [16], which is much higher than that of Portland cement ($b_{cm} = 5.5$ MJ/kg [16]). The embodied energy of insulation material is calculated similarly to Eq. (4) by,

$$B_m = b_m M_m = b_m \rho_m \frac{\pi}{4} \left(D_{wb}^2 - D^2 \right) L_m \tag{6}$$

where ρ_m is the density of the insulation material, 3400 kg/m^3 [21].

3. Modeling and analysis of flow and heat transfer in the wells

The underground system of deep EGS consists of at least one IW and one PW, and the stimulated reservoir. Section 2 provides the model for calculating the energy consumption for well construction. In pursuit of our objective (described in Section 1), the energy gains/losses of the geofluid and geofluid pumping energy demand are calculated. Energy gains/losses of geofluid are due to heat gain/loss from the IW/PW, and the geofluid pumping energy demand is proportional to the pressure changes. A model is therefore developed here to calculate the pressure and temperature changes of the geofluid flowing in the IW-s and PW-s. Knowledge of the pressure and temperature profile of the geofluid in the wells allows the determination of these energy components, and the effects of adding IW/PW, of enlarging their flow cross section areas and of adding thermal insulation to them. This produces the information needed for recommending a highest net energy output design of geothermal well systems.

Table 6
Well construction energy consumption results validation.

Well depth, km	This work, TJ	Ref. [19], TJ	Difference, %
5	80.2	84.0	−4.57
7.5	149.1	139.5	6.85
10	199.5	208.3	−4.24

3.1. The mathematical model for flow and heat transfer of geofluid

The assumptions are:

(1) For the purpose of this study it is not necessary to consider interactions between IW-s and PW-s, which are also typically far apart.
(2) The pressure is kept high enough to prevent the geofluid from evaporating.
(3) The time dependences of geofluid properties such as temperature, pressure, density, velocity and etc. are not included in the governing equations but are introduced in the dimensionless temperature parameter T_D (see Eqs. (21) and (22)). The heat transfer between the geofluid and the surrounding rock is therefore varying with time, and so are thus the geofluid temperature, pressure, velocity, and density and other fluid properties.
(4) The EGS geofluid is pure water devoid of gases and minerals. Water injected into an EGS reservoir often picks up various minerals and gases, but the associated complexity that is associated with their consideration in heat transfer analysis, accompanied by insufficient experimental information on their amount in various EGS systems, and since typically their content in the geofluid is low in EGS system, led most of the past studies to assume that the geofluid is pure [1,22–27].

Setting the mass flow rate of the injection geofluid to $\dot{m}_{iw}$, the mass flow rate of geofluid in each PW is:

$$\dot{m}_{pw} = \frac{(1 - r_{wl})\dot{m}_{iw}}{N_{pw}}, \tag{7}$$

where $\dot{m}_{iw/pw}$ is mass flow rate of the geofluid in a well, kg/s, r_{wl} is the geofluid loss rate in the reservoir (assumed to be 10% [1]) and N_{pw} is the number of PW-s per IW. So $N_{pw} = 1$ for doublet well-configuration, $N_{pw} = 3$ for quartet, etc.

Considering that the resistance pressure loss $\Sigma K V^2/2$ is minor compared to pipe friction loss $\Sigma 2fLV^2/D$ [28] for deep EGS wells where $L >> DK/4f$, the total pressure gradient during fluid flow is the sum of gravity, friction and the flow acceleration gradients [25,29]:

$$\frac{dP}{dz} + g\rho \mp f_D \frac{\overline{V}^2 \rho}{2D} + \rho \overline{V} \frac{d\overline{V}}{dz} = 0, \tag{8}$$

where the minus sign before f_D applies for IW-s and the plus sign applies for PW-s, and,

P – the geofluid pressure in wells, Pa;
z – the vertical position (along g) of the geofluid, m;
g – the gravitational acceleration, here 9.8 m/s^2;
ρ – the geofluid density in the wells, $\rho = \rho (P,T)$, kg/m^3 and T is the geofluid temperature, °C;
f_D – the Darcy friction factor;
$\overline{V}$ – the average flow velocity of the geofluid in the wells, m/s:

$$\overline{V} = \frac{4\dot{m}_{iw/pw}}{\pi \rho D^2} \tag{9}$$

Using Chen's explicit equation for Darcy friction factor f_D in pipes to simplify the calculation (this equation was reported to satisfy nearly the whole related range of Reynolds numbers (4×10^3 to 4×10^8) [30]):

$$f_D = \left[2 \log_{10} \left(\frac{\varepsilon/D}{3.7065} - \frac{5.0452}{\text{Re}} \log_{10} \Lambda \right) \right]^{-2}$$

$$\Lambda = \frac{(\varepsilon/D)^{1.1098}}{2.8257} + \left(\frac{7.149}{\text{Re}} \right)^{0.8981} \tag{10}$$

where:

ε — casing inner roughness factor, m;
Re — Reynolds number, $\text{Re} = \overline{V}D/\nu = \text{Re}\,(P,T)$, where ν is the kinematic viscosity of the geofluid, $\nu = \nu\,(P,T)$, m^2/s;

The specific enthalpy of the geofluid in the wells can be calculated from the energy balance equation [26]:

$$\frac{dh}{dz} + g + \overline{V}\frac{d\overline{V}}{dz} \mp \frac{\dot{Q}}{\dot{m}} = 0, \tag{11}$$

The minus sign in front of $\dot{Q}$ applies to IW-s and the plus sign applies to PW-s, and

h — specific enthalpy of geofluid, $h = h\,(P,T)$, J/kg;
$\dot{Q}$ — the heat transfer rate from surrounding rock to the geofluid per unit depth of wells, W/m. It is positive when the geofluid gains heat from the surrounding rock (in IW-s) while it is negative when it loses heat to the surroundings (in PW-s).

Using the heat transfer − electric resistance analogy (as shown in Fig. 4(b)), the heat transfer between the geofluid and surrounding rock has two thermal resistances in series: (1) Combined heat transfer from the geofluid to the wellbore/rock interface $1/U_1$, and (2) conduction heat transfer from the wellbore/rock interface to the undisturbed rock $1/U_2$ (the rock at some distance from wells where the temperature is undisturbed by the operation of wells).

The overall heat transfer coefficient from geofluid to wellbore/rock interface U_1 is calculated as:

$$\left(\frac{D_{wb}}{2} U_1 \right)^{-1} = \left(\frac{D}{2} h_f \right)^{-1} + \frac{\ln\left(\frac{D_{wb}}{D}\right)}{k_{cm}}. \tag{12}$$

where:

h_f − convection heat transfer coefficient between the geofluid and the casing inside surface, W/(m^2·K) [32]:

$$\frac{h_f D}{k} = 0.23\text{Re}^{0.8}\text{Pr}^{0.4} \tag{13}$$

k − thermal conductivity of the geofluid, $k = k\,(P,T)$, W/(m·K);
Pr − Prandtl number of the geofluid, $\text{Pr} = \text{Pr}\,(P,T)$;
k_{cm} − thermal conductivity of cement, here 0.29 W/(m·K) [20].

The thickness of casings is neglected here because it is less than 1% of the casing diameter [17], and since they are made of stainless steel, which has high heat conductivity relative to cement or rock (the ratio of conductivities of steel and cement is over 55 [20]). Therefore, the thermal resistance of the casings is neglected.
Assuming the temperature of the surrounding rock is a function of time τ and radial location r, an energy balance of the surrounding rock can be expressed in cylindrical coordinates as [32],

$$\frac{1}{\alpha_r}\frac{\partial T_r}{\partial \tau} = \frac{\partial^2 T_r}{\partial r^2} + \frac{1}{r}\frac{\partial T_r}{\partial r}, \tag{14}$$

where:

α_r − Thermal diffusivity of the surrounding rock, here 7.69×10^{-7} m^2/s [33];
T_r − temperature of surrounding rock at time τ and location r, W/(m·K);
τ − well operation time, s;
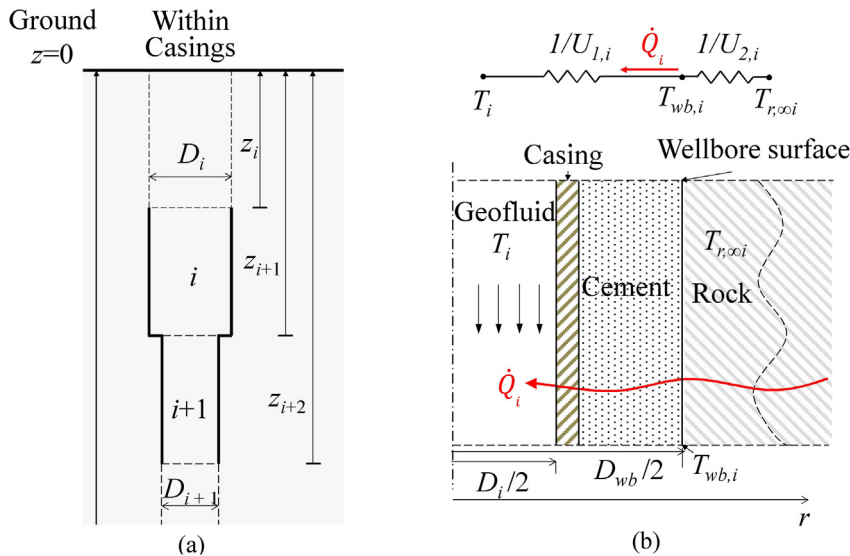r − distance from center of the well, m.

Fig. 4. (a) Sketch of well segment in the finite difference simulation scheme, and (b) the heat transfer process in the ith interval of an IW [31].

The initial condition is,

$$T_r(r, 0) = T_{r,\infty} \tag{15}$$

Based on the geothermal gradient, G, at the well site, the temperature of the undisturbed rock is,

$$T_{r,\infty} = T_s - z(G/1000). \tag{16}$$

The boundary conditions are,

$$\dot{Q} = \pi k_r D_{wb} \frac{\partial T_r}{\partial r}\bigg|_{r=D_{wb}/2} \tag{17}$$

$$\frac{\partial T_r}{\partial r}\bigg|_{r=+\infty} = 0$$

where k_r is the thermal conductivity of surrounding rock, here 1.61 W/(m·K) [33];

Defining a dimensionless temperature of the surrounding rock as,

$$T_D = -\frac{2\pi k_r}{\dot{Q}}(T_{wb} - T_{r,\infty}) \tag{18}$$

The continuity of heat flow yields [25],

$$\dot{Q} = \pi D_{wb} U_1 (T_{wb} - T) = -\frac{2\pi k_r}{T_D}(T_{wb} - T_{r,\infty}) \tag{19}$$

Eliminating T_{wb} in (19), we have,

$$\dot{Q} = \frac{2\pi D_{wb} U_1 k_r}{T_D D_{wb} U_1 + 2k_r}(T_{r,\infty} - T); \tag{20}$$

As derived in Refs. [34] and [27], an algebraic equation for T_D represents the solutions of Eqs. (14)–(17) quite accurately,

$$T_D = \ln\left[e^{-0.2t_D} + \left(1.5 - 0.3719e^{-t_D}\right)\sqrt{t_D}\right] \tag{21}$$

where t_D is the dimensionless well operation time [27]:

$$t_D = \frac{4\alpha_r \tau}{D_{wb}^2}; \tag{22}$$

As plotted in Fig. 5, T_D increases with t_D, indicating that a decreasing amount of heat $\dot{Q}$ is transferred to the geofluid in the wells from the rock because the geofluid temperature gradually rises due to the heat transfer from the surrounding rock, the rock temperature drops as it transfers its heat to the geofluid, and consequently the temperatures of the geofluid and rock approach each other over time until a steady state is reached.

3.2. The solution method, range and validation

A finite difference method is used to solve Eqs. (8) and (11), modeling a well composed of N longitudinal intervals, as shown in Fig. 4 (a). Fig. 4 (b) (modified from Ref. [31]) depicts the heat exchange with the surroundings in the ith interval of an IW. The geofluid flow and heat flow directions are reversed in PW-s.

Within each interval i, the geofluid is considered to be incompressible, with a constant density $\rho_i = \rho(P_i, T_i)$. All other geofluid thermal properties in each depth (z) interval i are evaluated at T_i and P_i. Eqs. (8) and (11) are thus expressed as [35]:

$$\frac{P_{i+1} - P_i}{\rho_i} + \frac{\overline{V}_{i+1}^2 - \overline{V}_i^2}{2} + g(z_{i+1} - z_i) \mp f_{Di}\frac{(z_{i+1} - z_i)\overline{V}_i^2}{2D_i} = 0$$
$$h_{i+1} - h_i + g(z_{i+1} - z_i) + \frac{\overline{V}_{i+1}^2 - \overline{V}_i^2}{2} \mp \frac{\dot{Q}_i(z_{i+1} - z_i)}{\dot{m}} = 0 \tag{23}$$
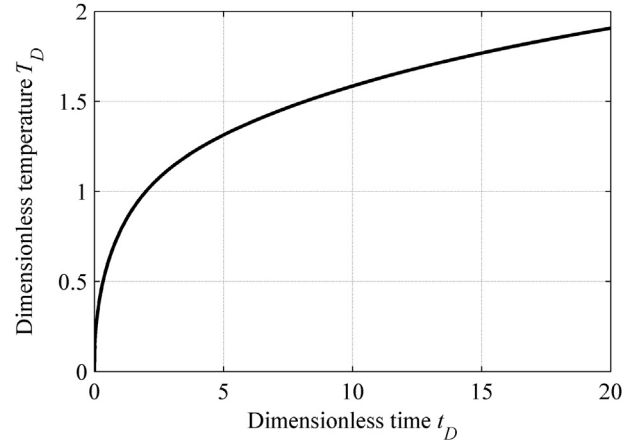

Fig. 5. The dimensionless temperature T_D as a function of the dimensionless well operating time t_D

The coupled finite difference Eq. (23) was solved by using the Engineering Equation Solver program (EES [36]). Simultaneous solution of Eq. (23) successively for each interval i leads to the determination of P_{i+1} and T_{i+1} from known P_i and T_i.

The surrounding rock is assumed to be granite. The geofluid properties are calculated in EES using its fluid property database 'Steam_IAPWS' [30]. All other used values are tabulated in the Nomenclature section at the end.

For validation of our analytical method, we first note that the conservation Eqs. (8) and (11) are consistent with the widely used ones in geothermal wellbore models GWELL, GWNACL, and HOLA [37,38]. Further validation, of the numerical results, was done by examining the effect of grid size on the resulting mass, pressure, and enthalpy balance, and choosing then a grid at which further size decreases have a negligible effect. For the validation, we chose the case of one 7.5 km deep PW with a geothermal gradient of 60 °C/km. The geofluid mass flow rate was assumed to be 100 kg/s. The geofluid at the wellhead is either saturated liquid or supercritical fluid at 23 MPa. The calculation procedure for the PW is shown in Fig. 6, where T_c is the critical temperature of pure water. The geofluid temperature at the PW well-bottom is assumed to be equal to the average reservoir temperature of 465 °C (Table 1). The calculation is to find the PW head geofluid temperature $T_{h,pw}$ and pressure $P_{h,pw}$, as well as the well-bottom pressure $P_{b,pw}$.

The resulting sensitivity of the numerical solution after 1 year of operation to grid size, where the size here is the well segment length, is shown in Fig. 7 (a). It can be seen that well segments length of 50 m is small enough to make the numerical solution essentially grid-size independent, and we therefore chose a well segments length of 25 m for all the computations in this study.

The numerical solutions were also tested by examining the magnitudes of the absolute mass, pressure, and enthalpy residuals of the governing Eq. (23).

$$R_{m,i} = \left| \dot{m}_{pm} - \frac{\overline{V}_i \pi \rho_i D_i^2}{4} \right|$$

$$R_{p,i} = \left| \frac{P_{i+1} - P_i}{\rho_i} + \frac{\overline{V}_{i+1}^2 - \overline{V}_i^2}{2} + g(z_{i+1} - z_i) + f_{Di}\frac{(z_{i+1} - z_i)\overline{V}_i^2}{2D_i} \right|,$$

$$R_{h,i} = \left| h_{i+1} - h_i + g(z_{i+1} - z_i) + \frac{\overline{V}_{i+1}^2 - \overline{V}_1^2}{2} + \frac{\dot{Q}_i(z_{i+1} - z_i)}{\dot{m}_{pw}} \right|$$
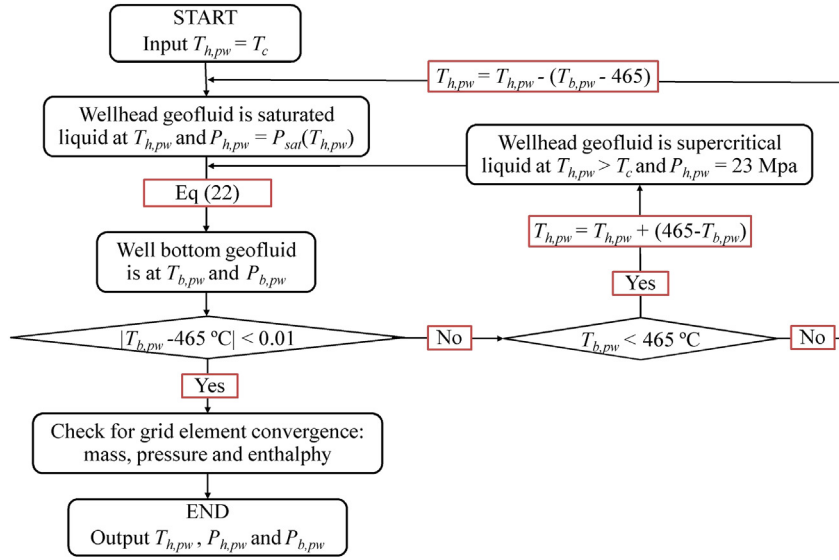
$$\tag{24}$$

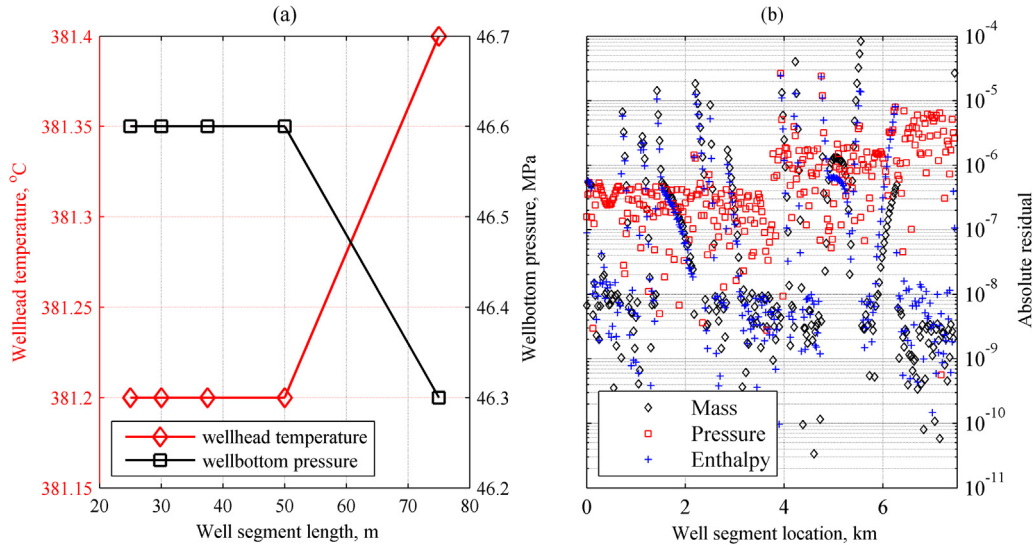Fig. 6. The calculation procedure diagram for the sample PW.

Fig. 7. (a) Grid size dependence of the PW wellhead temperature $T_{h,pw}$ and well bottom pressure $P_{b,pw}$; (b) numerical calculation residuals of flow in wells at the operation time of $\tau = 1$ yr.

Substituting all the values in Eq. (24) with the numerical calculation results, gives the residuals at each well segment i, presented in Fig. 7(b), which shows that the absolute residuals are all smaller than 10^{-4}, indicating a satisfactory and converged solution.

3.3. The time dependence of the results

Considering for example a 7.5 km deep PW with a geothermal gradient of 60 °C/km and geofluid flow rate of 100 kg/s the time variation of the wellhead temperature $T_{h,pw}$ and well bottom pressure $P_{b,pw}$ are shown in Fig. 8. The changes are rapid within the first year and then markedly slow down. The 40-year time-averaged wellhead temperature and well bottom pressure were calculated to be 381.5 °C and 46.5 MPa, respectively, which is approximately equal to the values after the operating time of 5

years. The results presented in the following sections are for the 40-year time-averaged values.

3.4. Results for injection wells

As described in Section 3.2, a 25 m long well segment was chosen for the finite difference analysis. The geofluid in the IW-s is kept as a supercooled liquid. The dynamic pressure change of geofluid in IW is defined as,

$$\Delta P_{d,iw} = P_{b,iw} - P_{h,iw} - \rho_{h,iw} g Z \qquad (25)$$

where $\rho_{h,iw}$ is the density (in kg/m^3) of the geofluid at IW head and it is a function of the IW head temperature $T_{h,iw}$. For the considered $T_{h,iw} = 35$ °C, 70 °C and 105 °C, the $\rho_{h,iw}$ is 994.0 kg/m^3, 977.8 kg/m^3 and 955.0 kg/m^3 [8], respectively.

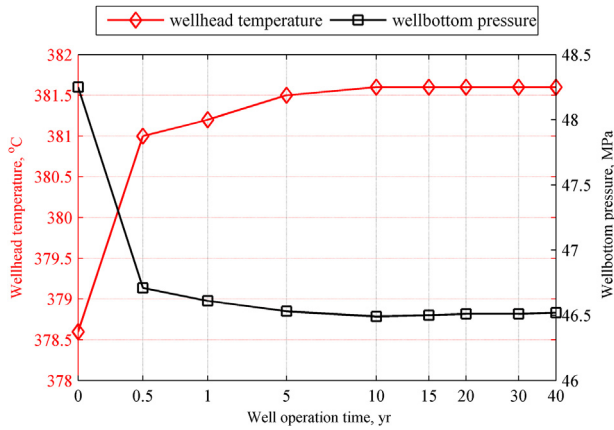The temperature change of geofluid in IW is defined as,

Fig. 8. Time variation of wellhead temperature $T_{h,pw}$ and well bottom pressure $P_{b,pw}$ in a 7.5 km deep PW with a geothermal gradient of 60 °C/km.

$$\Delta T_{iw} = T_{b,iw} - T_{h,iw} \tag{26}$$

Fig. 9 presents the results of a sensitivity analysis of $\Delta P_{d,iw}$ and ΔT_{iw} to six parameters, the well depth Z, geothermal gradients G, geofluid flow rate $\dot{m}_{iw}$, well relative flow cross section area A^*, geofluid injection temperature $T_{h,iw}$ and geofluid injection pressure $P_{h,iw}$. Their chosen values are presented in Table 7.

The following conclusions can be drawn from the results presented in Fig. 9:

(1) The dynamic pressure change $\Delta P_{d,iw}$ rises with decreased flow rate $\dot{m}_{iw}$ and increased well relative flow cross section area A^* because of decreased friction pressure loss in both cases. The well depth Z, geothermal gradient G, injection temperature and $T_{h,iw}$ and pressure $P_{h,iw}$ have negligible effect on the dynamic pressure change (the symbols in the plots of Fig. 9 overlap).

(2) The temperature change ΔT_{iw} rises with increased well depth Z and geothermal gradient G because hotter rock transfers heat to the geofluid. The temperature change rises with decreased flow rate $\dot{m}_{iw}$ because the heat gained from rock per unit geofluid mass increases. It also slightly rises with the decreased well relative flow cross section area A^* because the decrease of well bottom geofluid pressure (caused by friction) over-compensates the decrease of well bottom geofluid
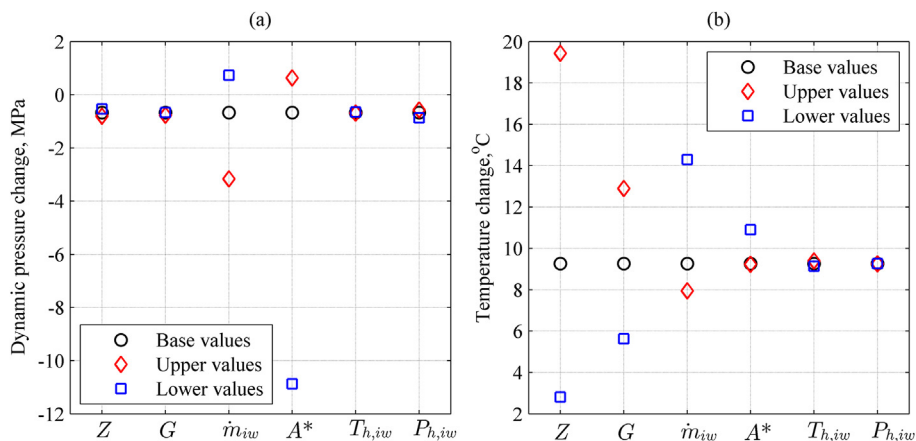
enthalpy (caused by reduced geofluid and rock heat transfer area), resulting in a slightly increased geofluid temperature.

Regression of the resulting data produces the following approximate equations to express the well bottom pressure $P_{b,iw}$ and temperature $T_{b,iw}$ as a function of the studied parameters:

$$P_{b,iw} \cong P_{h,iw} + \rho_{h,iw} g Z - C_1 \left(\frac{\dot{m}}{A^*} \right)^{C_2} - C_3$$

$$T_{b,iw} \cong T_{h,iw} + C_4 Z \cdot G + C_5 \dot{m} + C_6 \tag{27}$$

where $C_1 = 4.87 \times 10^{-7}$ s^{C_2}/kg^{C_2}, $C_2 = 3.13$, $C_3 = 0.9$ MPa, $C_4 = 2.26 \times 10^{-2}$, $C_5 = -4.87 \times 10^{-7}$ s/kg and $C_6 = 16.84$ °C.

3.5. Results for production wells

The PW bottom temperature is assumed to be equal to the average temperature of the reservoir (Table 1). The pressure of the geofluid is continuous in the EGS system, as shown in the explanatory schematic Fig. 10. The PW head pressure $P_{h,pw}$ is the lowest in the subsurface system, which needs to be kept high enough to maintain the geofluid in saturated liquid ($P_{h,pw} = P_{sat}(T_{h,pw})$) or supercritical state ($P_{h,pw} = 23$ MPa, ~1 MPa above the critical pressure of water). The arrows in Fig. 10 indicate the flow direction of the geofluid. The pressure change to be provided by the injection pump is:

$$\Delta P_{ip} = \Delta P_{pw} - \Delta P_{iw} + \Delta P_r + \Delta P_{pp}, \tag{28}$$

where:

ΔP_{pw} — the geofluid pressure drop in PW-s, $\Delta P_{pw} = P_{b,pw} - P_{h,pw}$, MPa, calculated using Eq. (23).
ΔP_{iw} — the geofluid pressure change in the IWs, MPa. $\Delta P_{iw} = P_{b,iw} - P_{h,iw}$, calculated using Eq. (27).
ΔP_r — the geofluid pressure drop in the fractured reservoir, MPa. It is a function of reservoir depth, geothermal gradient and the characteristics of reservoir fractures including the number of fractures, fracture radius, fracture width and permeability [3].
ΔP_{pp} — the geofluid pressure drop in the power plant, MPa. For flash and supercritical power plants analyzed by us in Ref. [8], the pump within the power plant is to bring the geofluid to the pressure at which it enters the plants. For a binary power plant, the geofluid exchanges heat with a secondary working fluid in a

Fig. 9. (a) Geofluid dynamic pressure change and (b) temperature change in IW with respect to the well depth Z, geothermal gradients G, geofluid flow rate $\dot{m}_{iw}$, well relative flow cross section A^*, geofluid injection temperature $T_{h,iw}$ and geofluid injection pressure $P_{h,iw}$.

Table 7
Chosen values for the IW $\Delta P_{d,iw}$ and ΔT_{iw} sensitivity analysis.

	Well depth Z, km	Geothermal gradients G, °C/km	Flow rate $\dot{m}_{iw}$, kg/s	Well relative flow cross section area A^*	Injection temperature $T_{h,iw}$, °C	Injection pressure $P_{h,iw}$, MPa
Upper values	11.3	90.0	166.7	1.5	105.0	15.0
Base values	7.5	60.0	111.1	1.0	70.0	10.0
lower values	3.8	30.0	55.6	0.5	35.0	5.0

heat exchanger. The pressure drop in the heat exchanger is relatively small and assumed to be negligible [2]. Therefore,

$$\Delta P_{pp} = 0. \tag{29}$$

The energy output (in TJ) from the EGS well system is the net electricity output of the geothermal power plant minus the required pumping energy due to the frictions in the wells, over its lifetime,

$$E_{out} = \left(E_{pp} - \frac{(\Delta P_{pw} - \Delta P_{iw})\dot{m}_{iw}}{\bar{\rho}_{ip}\eta_p} \right) FL_f, \tag{30}$$

where:

E_{pp} — the net power output from the surface power plant, MJ. It is an increasing function of PW head temperature $P_{h,pw}$ (equivalent to power plant inflow geofluid temperature) and is fitted using the results presented in our paper [8], as follows:

$$E_{pp} = 5.0 \times 10^{-5} T_{h,pw}^{2.6466} \sum_1^{N_{pw}} \dot{m}_{pw}, \ T_{h,pw} \in [200°C, \ T_c]$$

$$E_{pp} = \left(937.78 \ln\left(T_{h,pw}\right) - 4815.5 \right) \sum_1^{N_{pw}} \dot{m}_{pw}, \ T_{h,pw} \in (T_c, 800°C]$$
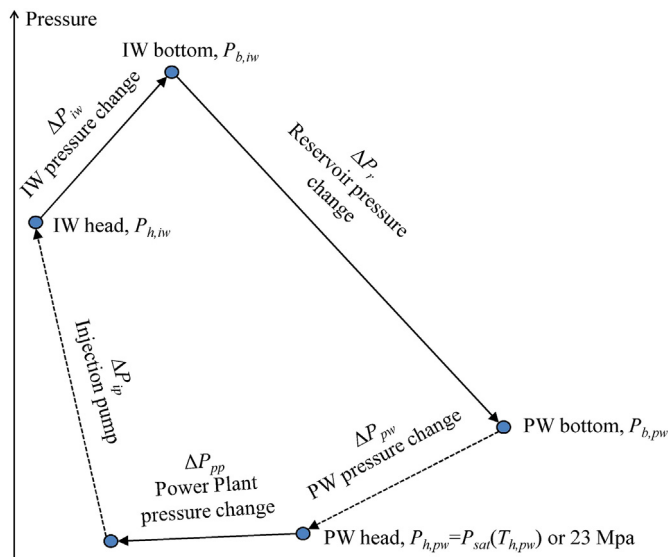
$$\tag{31}$$

Fig. 10. Explanatory schematic of the pressure profile in the EGS system.

ρ_{ip} — the density of the geofluid flowing through the injection pump. Assumed to be 977.8 kg/m^3 [36] because the geofluid injection temperature is approximately 70 °C [8];

η_p — the energy efficiency of the injection pump, assumed here to be 80%;

F — the capacity factor of the surface geothermal power plant, assumed to be 70% [39];

L_f — the life of EGS well system, assumed to be 40 years [3].

The 40-yrs-averaged PW head temperature $T_{h,pw}$ and pressure drop ΔP_{pw} as well as IW pressure drop ΔP_{iw} are used in Eqs. (30) and (31) to calculate E_{out}.

To increase the energy output E_{out}, the design of PW-s should either increase the PW head geofluid temperature $T_{h,pw}$ or decrease the pressure drop in PW-s ΔP_{pw} (Eq. (30)). The geofluid pressure drop in PW-s, ΔP_{pw}, for a given flow cross section area can be reduced by reducing the mass flow rate in a well to reduce the friction pressure loss. To attain a chosen overall hot geofluid extraction rate, the number of such wells needs to be increased. Another way to reduce the friction pressure loss is to increase the flow cross section area of the wells for the same flow rate. The PW head geofluid temperature $T_{h,pw}$ can be increased by reducing the heat loss from the hot geofluid to the surrounding rock, e.g., by replacing the cement between the casing outer surface and the rock by thermal insulation materials, such as ceramic insulation (that has high temperature resistance).

3.5.1. Effects of increasing the number of PW-s

The geofluid pressure drop in PW-s, ΔP_{pw}, and temperature at the PW head, $T_{h,pw}$, for different numbers of PW-s and whether insulation is incorporated are plotted in Fig. 11, for different well depths and geothermal gradients. As mentioned, the total mass flow rate of the geofluid in the PW-s was assumed to be 100 kg/s.

The pressure drop ΔP_{pw} decreases with increased geothermal gradients because of the increased buoyancy effect when the geofluid becomes hotter. Fig. 11 also shows that insulation has little effect on the pressure drop, while the number of PW-s has large effect on the pressure drop. For deeper wells ($\geq$7.5 km) with larger geothermal gradients ($\geq$60 °C/km), adding more PW-s can reduce the pressure drop by over 60%.

The insulation could increase $T_{h,pw}$ but the degree of improvement is less than 10 °C. Adding more PW-s will increase $T_{h,pw}$ because reduced geofluid velocity reduces the convective heat loss (Eq. (13)) to the surrounding rock.

3.5.2. Effects of increasing the flow cross section area of PW-s

As mentioned, another way to reduce the pressure drop in a PW is to increase its flow cross section area. While this may be difficult due to the cost and even technology limitations, we analyze this option here to examine the potential resulting improvements. The following results are calculated by solving Eq. (23) with enlarged flow cross section areas.

The computed geofluid pressure drop in PW-s, ΔP_{pw}, and PW head geofluid temperature $T_{h,pw}$ for PW-s with different cross section areas and whether insulation is incorporated are plotted in Fig. 12 for different well depths and geothermal gradients. As
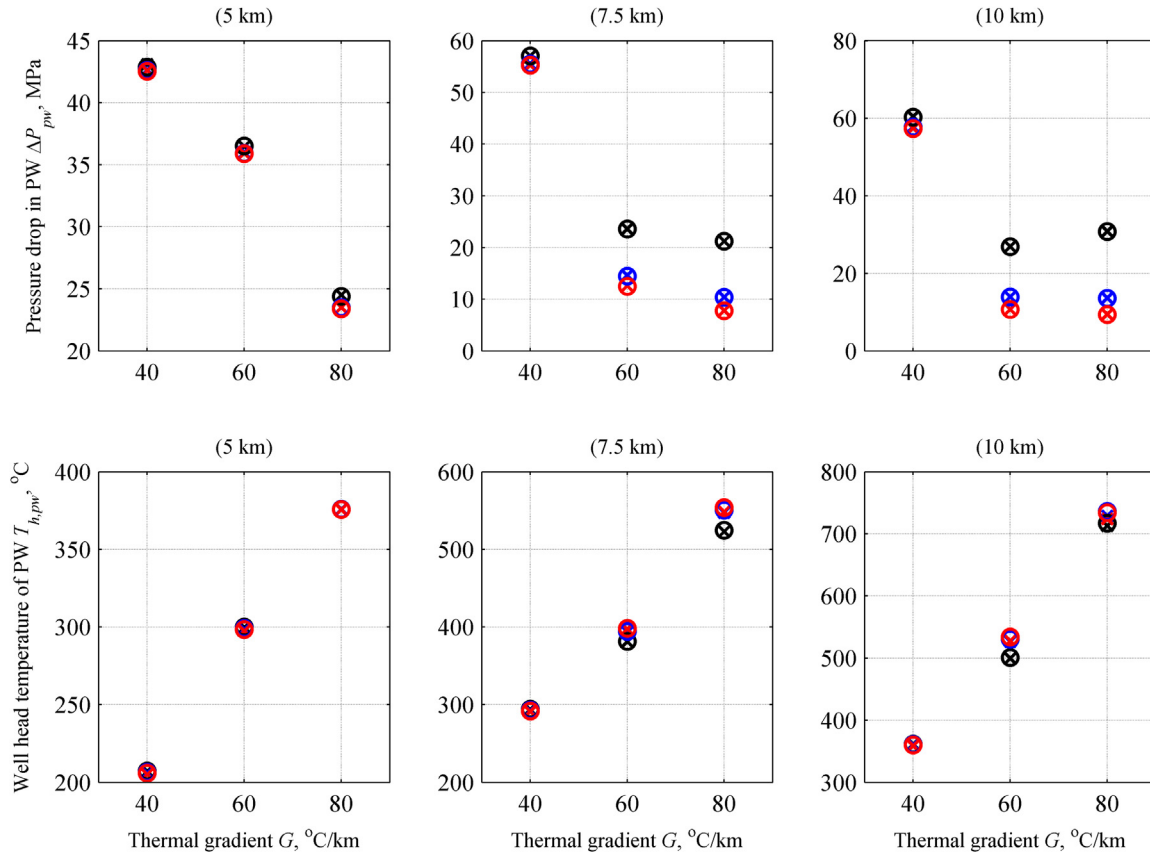
Fig. 11. The geofluid pressure drop ΔP_{pw} in PW-s (top row) and the geofluid temperature $T_{h,pw}$ at PW head (bottom row) of different numbers of PW-s and whether insulation is incorporated. The black symbols: $N_{pw} = 1$, blue symbols: $N_{pw} = 2$, red symbols: $N_{pw} = 3$. The crosses 'x': no insulation is incorporated, circles 'o': the insulation is incorporated. (For interpretation of the references to color in this figure legend, the reader is referred to the web version of this article.)

shown in Fig. 12, the effect of insulation on the pressure drop was found to be very small, but the flow cross section areas of PW-s have large effect on the pressure drop. For deeper wells (≥ 7.5 km) with larger geothermal gradients (≥ 60 °C/km), enlarging the flow cross sections areas of PW-s was found here to reduce the pressure drop by over 60%.

The insulation could increase $T_{h,pw}$ but by less than 8 °C. Enlarging the flow cross section areas of PW-s increases $T_{h,pw}$ because reduced geofluid velocity reduces the convective heat loss (Eq. (13)) to the surrounding rock.

Comparison of Fig. 11 to Fig. 12 shows that the effects of enlarging the well flow cross section area and those of drilling more wells, on PW pressure drop and PW head temperature, are similar.

4. Design guidance for well system

The design guidance for well systems is based on net-energy and *EROI* (energy return on investment) performance criteria, as presented in this section.

4.1. Net-energy-based design guidance for PW systems

Improving system energy performance by increasing the number of PW-s or increasing their flow cross section areas, or by insulating them from the surrounding rock, consumes more energy to construct. Suitable thermal insulation materials (such as magnesia) are much more expensive than cement, and their specific embodied energy is much higher than that of Portland cement (Section 2.4). An optimal energy-based design would thus take into

account the increase of the energy output E_{out} (TJ) as a result of such changes as well as the corresponding energy input E_{in} (TJ) needed to construct them, and this are calculated below, noting that the energy input of preparing the drilling site as well as setting the drilling rigs have however not been included. The total energy input (Section 2.4) to construct the EGS well system is,

$$E_{in} = (N_{pw} + 1)E_{well} + N_{pw}I_m(B_m - B_{cm}), \tag{32}$$

where:

E_{well} — energy consumed to construct one well, TJ, which is given in Section 2.4.

I_m — indicator of whether the cement of PW-s is replaced with insulation material to reduce heat loss to surrounding rock; $I_m = 1$ when cement is replaced with insulation material while $I_m = 0$ when cement is not replaced with insulation material.

The net energy output of EGS well system is listed in Table 8 and defined as,

$$E_{net} = E_{out} - E_{in} \tag{33}$$

The chosen performance criterion for comparison is the relative net energy increment for case j, $(\Delta E_{net}^j)_R$, defined as,

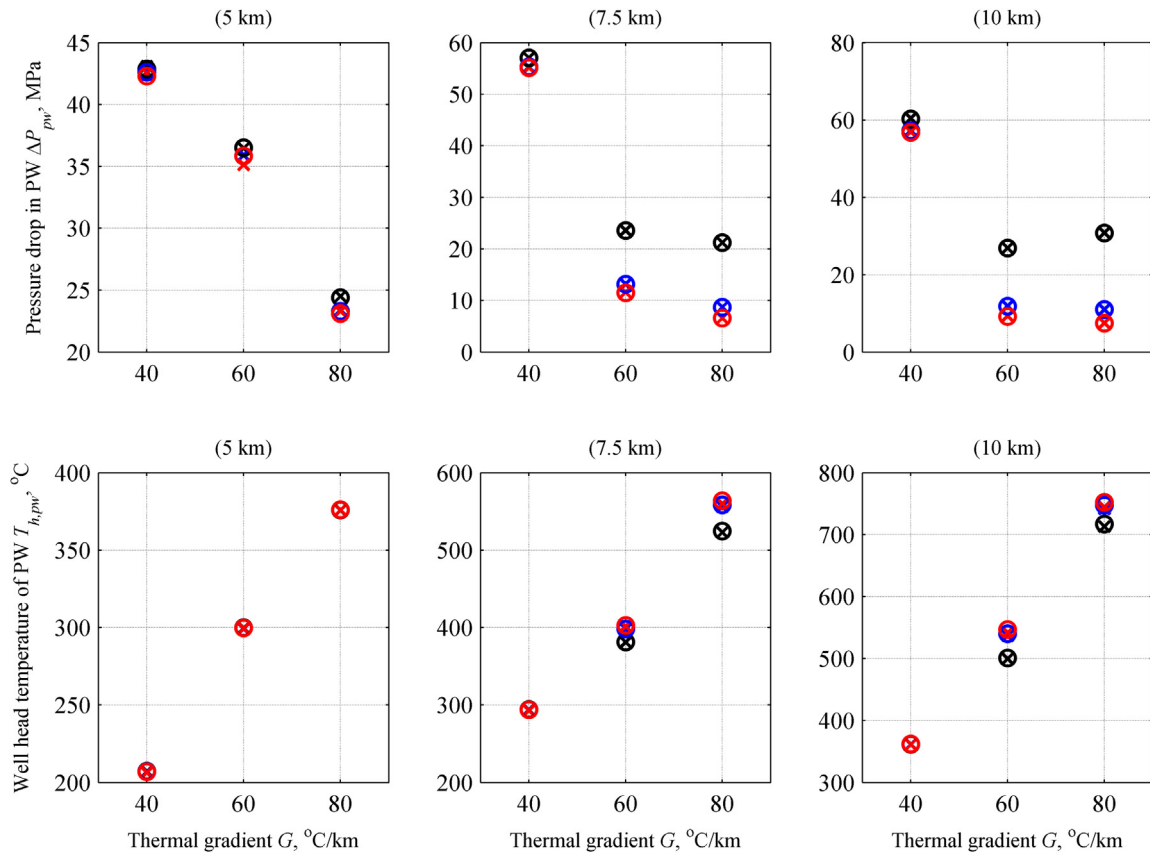$$\left(\Delta E_{net}^j\right)_R \equiv \frac{E_{net}^j - E_{net}^{base}}{E_{net}^{base}} \tag{34}$$

Fig. 12. The geofluid pressure drop in PW-s ΔP_{pw} (top row) and the geofluid temperature $T_{h,pw}$ at PW head (bottom row) of different PW flow cross section areas and whether insulation is incorporated. The black symbols: $A^* = 1$, the blue symbols: $A^* = 2$ and the red symbols: $A^* = 3$. The crosses 'x': no insulation is incorporated and the circles 'o': the insulation is incorporated. (For interpretation of the references to color in this figure legend, the reader is referred to the web version of this article.)

where the chosen base design is D0, which is a single PW with $A^* = 1$ using Portland cement casing. Cases D1 to D9 correspond to designs with different numbers of PW-s, different flow cross sections of PW-s and replacement of the Portland cement by magnesia insulation. Comparison in Table 8 of the results for D1 vs. D6, D2 vs. D7, D4 vs. D8, and D5 vs. D9, shows that enlarging the well cross sections raises the net energy output only by 0.05%–2.43% more than adding more wells for the same total geofluid output flow rate (assumed to be 100 kg/s).

In this comparative study of 10 different PW system designs, the highest net energy output designs characterized by largest positive $(\Delta E_{net})_R$ are shown in bold underlined font in Table 8 and are listed in Table 9. Use of the magnesia insulation increases the energy output from the 40 °C/km resource with 5 km deep wells, the 60 °C/km resource with 5 km and 10 km deep wells, and the 80 °C/km resource with 7.5 km and 10 km deep wells, because the heat loss from the geofluid to surrounding rock in PW-s is significant. For the resource with 40 °C/km geothermal gradient, the highest net energy output design of PW-s system is single 10 km PW with cross section doubled as compared to Fig. 2, and without magnesia insulation. For a resource with 60 °C/km gradient, the recommended design is single 10 km PW with tripled cross section, and with magnesia insulation. For a resource with 80 °C/km gradient, the recommended design is single 7.5 km PW with cross section tripled, and with magnesia insulation.

Table 9 presents the corresponding geofluid pressure drop in the PW-s ΔP_{pw}, the geofluid temperature at PW head $T_{h,pw}$, and the geofluid temperature drop in the PW-s, ΔT_{pw} ($\Delta T_{pw} = T_{b,pw} - T_{h,pw}$) of the highest net energy output designs. The asterisked numbers

in Table 9 indicate when the produced geofluid is supercritical. Table 9 shows that when the geothermal gradient is 40 °C/km for 5 km–10 km deep wells, and 60 °C/km for the 5 km deep well, the produced geofluid is at saturated liquid phase, and under the other conditions the produced geofluid is in the supercritical phase.

The pressure drop in PW-s ΔP_{pw}, decreases with higher geothermal gradient because of the increased assistance from buoyancy of the geofluid. The values of ΔP_{pw} are much smaller for supercritical geofluid than for saturated geofluid because of its larger density variation.

The temperature drop in PW-s ΔT_{pw} increases with increased well depths and geothermal gradients because of the corresponding increased area and consequent heat loss to the surrounding rock, and larger acceleration energy. The acceleration energy component in Eq. (11) (the 3rd term) is larger because the velocity increases due to decreased density of the geofluid for hotter resources.

The temperature at PW head, $T_{h,pw}$, is the geofluid inflow temperature to the power plant, from which the net electricity generation from power plant can be calculated using Eq. (31).

4.2. EROI-based design guidance for PW systems

The *EROI* (energy return on investment), defined as the life-time ratio of the energy output of an energy conversion system relative to the energy required to construct it, is an important and widely used performance criterion, so we have calculated it for the EGS well systems considered in this study. Specifically for the well system *j*, the *EROI* is defined as:

Table 8

Net energy output (E_{net}) and relative (($\Delta E_{net})_R$) differences for 10 designs over the lifetime of wells (40 years). Bolded underlined numbers show the maximal positive E_{net} and ($\Delta E_{net})_R$. Asterisked numbers show the maximal positive E_{net} and ($\Delta E_{net})_R$ for a given geothermal gradient.

Geothermal gradient G, °C/km				40			60			80		
Well depth Z, km				5	7.5	10	5	7.5	10	5	7.5	10
Design#	N_{pw}	I_m	A^*	Net energy output E_{net}, PJ								
D0	1	0	1	6.39	16.50	29.99	17.10	72.61	97.51	68.53	99.10	126.49
D1	2	0	1	6.29	16.32	29.90	16.92	76.24	103.30	68.57	104.06	130.28
D2	3	0	1	6.14	16.07	29.49	16.70	77.11	103.69	68.45	104.42	130.04
D3	1	1	1	**<u>6.41</u>**	16.48	29.96	**<u>17.11</u>**	72.54	97.67	68.53	99.26	126.83
D4	2	1	1	6.26	16.27	29.83	16.96	76.22	103.69	68.52	104.41	130.86
D5	3	1	1	6.11	15.89	29.37	16.74	77.11	104.34	68.40	104.95	130.84
D6	1	0	2	6.34	**<u>16.51</u>**	30.18*	17.05	77.33	105.14	**<u>68.61</u>**	105.58	132.03
D7	1	0	3	6.26	16.31	29.97	17.08	**<u>78.19</u>**	106.06	68.54	106.30	132.56
D8	1	1	2	6.31	16.44	30.08	17.05	77.26	105.44	68.59	105.80	132.45
D9	1	1	3	6.23	16.19	29.80	16.92	78.16	**<u>106.48*</u>**	68.50	**<u>106.57</u>**	**<u>133.08*</u>**
				Relative net energy output increments ($\Delta E_{net})_R$, %								
D0	1	0	1	0.00	0.00	0.00	0.00	0.00	0.00	0.00	0.00	0.00
D1	2	0	1	−1.54	−1.14	−0.27	−1.02	5.00	5.94	0.07	5.01	3.00
D2	3	0	1	−3.85	−2.64	−1.65	−2.33	6.21	6.34	−0.12	5.37	2.81
D3	1	1	1	**<u>0.24</u>**	−0.16	−0.10	**<u>0.09</u>**	−0.09	0.17	0.00	0.16	0.27
D4	2	1	1	−2.00	−1.41	−0.52	−0.80	4.97	6.34	0.00	5.36	3.46
D5	3	1	1	−4.36	−3.71	−2.05	−2.12	6.20	7.01	−0.19	5.91	3.44
D6	1	0	2	−0.79	**<u>0.02</u>**	0.63*	−0.30	6.51	7.82	**<u>0.12</u>**	6.54	4.38
D7	1	0	3	−2.10	−1.19	−0.06	−0.13	**<u>7.69</u>**	8.77	0.02	7.27	4.80
D8	1	1	2	−1.25	−0.42	0.32	−0.26	6.41	8.13	0.10	6.77	4.71
D9	1	1	3	−2.57	−1.90	−0.64	−1.02	7.65	**9.20***	−0.03	**7.54***	**<u>5.22</u>**

$$EROI_j = \frac{E^j_{out}}{E^j_{in}} \qquad (35)$$

where E^j_{out} is the power output from the EGS system j, as calculated from Eq. (30), and E^j_{in} is the energy input needed to construct the well system j, as calculated by Eq. (32).

The relationship between $EROI$ and ($\Delta E_{net})_R$ for each Design j can be derived from Eqs. (33)—(35) as:

$$EROI_j = E^{base}_{net} \left(\frac{(\Delta E^j_{net})_R + 1}{E^j_{in}} \right) + 1 \qquad (36)$$

Since E^{base}_{net} is a selected positive constant, Eq. (36) shows that the $EROI_j$ of EGS well system j increases with the ratio of the relative net energy increment for case j as ($\Delta E^j_{net})_R$, which represents an energy efficiency for that system relative to the base-case in the energy comparison sample (Table 8), to the total energy input to construct this EGS well system j, E^j_{in}, thus from Eq. (36) as $[(\Delta E^j_{net})_R + 1]/E^j_{in}$. This explains why the values of $EROI_j$ (Table 10) were found to decrease even when the values of ($\Delta E^j_{net})_R$ (Table 8) were positive, simply the value of the energy input E^j_{in} in all these cases rose by more than the rise in $[(\Delta E^j_{net})_R + 1]$.

To avoid misunderstanding, it is noteworthy that the $EROI$ and the 'relative net energy increment' ($\Delta E_{net})_R$, used in Section 4.1, have different definitions and purposes: the former is absolute for a given well system, while the latter is comparative among a selected sample of different well systems.

The $EROI$ was found to decrease with the increase of the number of PW-s and with the increase of their flow cross section areas, because the required energy input E_{in} of design D0 is substantially lower than for the other designs, while its energy output E_{out} is relatively just a little lower. For example, doubling the number of PWs or doubling the cross section of a PW will approximately double the required energy input E_{in}, but the corresponding increase of energy output E_{out} is less than 8%. Replacement of regular cement by Magnesia insulation decreases the EROI for the same reason.

Table 10 shows that the simplest design, D0, with a single production well of the smallest considered flow cross section and no thermal insulation has the highest $EROI$ in comparison with all the proposed and analyzed alternatives D1 − D9. While many of these alternative designs raise the well systems energy output E_{out}, the energy input E_{in} required to construct them was found to increase relatively more. It is noteworthy, however, that employment of more energy efficient drilling methods and materials of lower embodied energy can lead to designs employing the proposed improvement approaches that would also have a larger $EROI$.

5. Conclusions

The objective of this study is to examine quantitatively the energy input and output for typical EGS well systems up to 10 km deep and by developing models and using them to analyze various

Table 9

The highest net energy output designs of PW system for different well depths and geothermal gradients. Asterisked numbers indicates that the geofluid is supercritical.

Geothermal gradient G, °C/km	40			60			80		
Well depth Z, km	5	7.5	10	5	7.5	10	5	7.5	10
# of PWs	1	1	1	1	1	1	1	1	1
I_m	1	0	0	1	0	1	0	1	1
A^*	1	2	2	1	3	3	2	3	3
ΔP_{pw}, MPa	42.9	55.3	57.3	36.5	11.6	9.2	23.4	6.6	7.5
ΔT_{pw}, °C	7.7	21.7	53.6	15.0	83.7	68.1	39.1	51.3	62.8
$T_{h,pw}$, °C	207.3	293.3	361.4	300.0	381.3*	546.9*	375.9*	563.7*	752.2*

Table 10
Energy return on investment EROI for 10 designs over the lifetime of wells (40 years).

Geothermal gradient G, °C/km				40			60			80		
Well depth Z, km				5	7.5	10	5	7.5	10	5	7.5	10
Design#	N_{pw}	I_m	A^*	Energy return on investment, EROI								
D0	1	0	1	40.8	56.3	76.2	107.6	244.5	245.4	428.2	333.3	318.0
D1	2	0	1	27.1	37.5	51.0	71.3	171.4	173.6	286.0	233.6	218.7
D2	3	0	1	20.2	27.9	38.0	53.1	130.3	130.9	214.4	176.1	164.0
D3	1	1	1	33.8	43.5	58.8	88.6	188.1	189.5	351.6	257.0	245.7
D4	2	1	1	21.2	27.0	36.6	55.6	122.7	124.9	221.5	167.7	157.4
D5	3	1	1	15.3	19.4	26.4	40.3	90.2	91.3	161.6	122.3	114.2
D6	1	0	2	27.3	37.9	51.4	71.9	173.9	176.7	286.2	237.0	221.6
D7	1	0	3	20.5	28.3	38.6	54.2	132.1	133.9	214.7	179.2	167.1
D8	1	1	2	21.3	27.2	36.9	55.9	124.4	127.0	221.7	169.9	159.3
D9	1	1	3	15.6	19.7	26.8	40.7	91.4	93.1	161.8	124.2	116.2

ways to improve the well-system energy performance. The main results include:

- The well construction energy consumption was found to be 19.40 TJ/(km of well) for wells with flow cross sections recommended in Ref. [11], and it increases approximately linearly with the increase of the well flow cross section area.
- The associated embodied energy requirement was found to be about 43.0%–49.8% of the total energy requirement.
- A correlation equation was developed to express the injection wells' bottom pressure $P_{b,iw}$ as a function of the injection pressure $P_{h,iw}$, well depth Z, mass flow rate $\dot{m}_{iw}$ and well relative flow cross section area A^*.
- A correlation equation was developed to express the IW bottom temperature $T_{b,iw}$ as a function of the injection temperature $T_{h,iw}$, well depth Z, geothermal gradient G and mass flow rate $\dot{m}_{iw}$.
- The pressure drop in a PW decreases with increased geothermal gradients because of the increased flow-supporting buoyancy effect when the geofluid becomes hotter.
- Adding insulation to PW-s has little effect on the pressure drop in PW but can increase the wellhead temperature by 8–10 °C.
- The number of PW-s and their flow cross section areas have a strong effect on the geofluid pressure drop in a PW: e.g., for deeper wells ($\geq$7.5 km) with larger geothermal gradients ($\geq$60 °C/km), adding more PW-s or enlarging their flow cross section areas can reduce the pressure drop by over 60%.
- Adding more PW-s or enlarging their flow cross section areas will increase $T_{h,pw}$ because the reduced geofluid velocity reduces the convective heat loss to the surrounding rock.
- Constructing wells with larger flow cross section areas has only 0.05%–2.43% more net energy output than constructing more wells.
- It is advantageous to add insulation to PW-s when (1) $G = 40$ °C/km, $Z = 5$ km, (2) $G = 60$ °C/km, $Z = 5$ km or 10 km and (3) $G = 80$ °C/km, and $Z = 7.5$ km or 10 km.
- Single 10 km deep production wells with doubled flow cross section are recommended for a 40 °C/km resource. Single 10 km deep production wells with tripled flow cross section and insulation are recommended for a 60 °C/km resource, and single 7.5 km deep production wells with tripled flow cross section and insulation are recommended for an 80 °C/km resource.
- Supercritical geofluid will be produced for (1) $G = 60$ °C/km, $Z = 7.5$ km or 10 km and (2) $G = 80$ °C/km, and $Z \geq 5$ km.
- The *EROI* was found to decrease with the increase of the number of PW-s, with the increase of their flow cross sections and the addition of insulation, because the energy input in all these cases rose relatively more than did the resulting energy output. Employment of more energy efficient drilling methods and materials of lower embodied energy can, however, lead to

designs employing the proposed improvement approaches that would also have a larger *EROI*. The design with a single PW, smallest cross section with no insulation had the largest *EROI*
- The considered EGS well systems have EROI of 33.8–286.2.

Nomenclature and abbreviations

All the values of thermal properties listed below are evaluated at the average temperature in the considered temperature range.

Parameters related to the construction energy consumption of wells (Section 2)

Symbol, name, value and unit

A^*	relative flow cross section area
B_{cm}	embodied energy of the cement, TJ
B_{cs}	embodied energy of the casings, TJ
B_m	embodied energy of the magnesia insulation, TJ
b_{cm}	specific embodied energy of cement, 5.5 MJ/kg [16]
b_{cs}	specific embodied energy of casing, 56.7 MJ/kg [16]
b_m	specific embodied energy of magnesia insulation, 45.0 MJ/kg [16]
D	the diameter of casing, m
D_{wb}	the diameter of wellbore, m
$\dot{E}_{dr}$	daily chemical energy consumption, 0.384 TJ/day[11,14]
E_{dr}	energy consumption of creating boreholes, TJ
E_{other}	the other energy consumption of drilling, TJ
E_{well}	energy consumption of constructing wells, TJ
e_{well}	specific energy consumption of wells, TJ/km
I_m	indicator of whether cement is replaced with magnesia insulation
L_c	casing length/cementing length, m
L_{dr}	drilling distance, m
M_m	mass of magnesia insulation, kg
M_{cm}	mass of cement, kg
M_{cs}	mass of casing, kg
Z	well depth, km
ρ_{cm}	density of cement, 1522 kg/m^3 [18]
ρ_m	density of magnesia insulation, 3400 kg/m^3 [21]

Parameters related to the flow and heat transfer of geofluid in wells (Section 3)

Symbol, name, value and unit

F	capacity factor of surface power plant, 70% [39]
f_D	the Darcy friction factor

G the average geothermal gradient, °C/km

g the gravitational acceleration, 9.8 m/s^2

h the specific enthalpy of geofluid, J/kg

h_f convection heat transfer coefficient between geofluid and casing inside surface, W/(m$^2 \cdot$K)

k thermal conductivity of geofluid, W/(m$\cdot$K)

k_{cm} thermal conductivity of cement, 0.29 W/(m$\cdot$K) [20]

k_m thermal conductivity of magnesia insulation, 0.07 W/(m$\cdot$K) [20]

k_r thermal conductivity of surrounding rock, 1.61 W/(m$\cdot$K) [33]

L_f lifetime of wells, 40 yrs [3]

$\dot{m}_{iw/pw}$ mass flow rate of geofluid in each IW/PW, kg/s

N the number of longitudinal intervals of a wellbore

P the geofluid pressure in wells, Pa

Pr   Prandtl number of geofluid

$\dot{Q}$ heat transfer rate from surrounding rock to the geofluid per unit length of wells, W/m

Re   the Reynolds number

R_h absolute residual of energy conservation equation, J/kg

R_m absolute residual of mass flow rate conservation equation, kg/s

R_p absolute residual of pressure conservation equation, Pa

r distance from center of the well, m

r_{wl} the geofluid mass loss rate in reservoir, 10% [1]

T the geofluid temperature in wells, °C

T_c the critical temperature of pure water, 374.1 °C [40]

T_D dimensionless temperature

t_D dimensionless well operation time

T_s the ground surface temperature, 15 °C [6]

T_r the temperature of rock, °C

$T_{r,\infty}$ the temperature of undisturbed rock, °C

T_{wb} the temperature of wellbore/rock interface, °C

U_1 overall heat transfer coefficient, W/(m$^2 \cdot$K)

$\overline{V}$ the average flow velocity of geofluid in wells, m/s

z the vertical position of geofluid, m

α_r thermal diffusivity of surrounding rock, 7.69×10^{-7} m^2/s [33]

ΔP_{pp} geofluid pressure drop in surface power plant, 0 Pa [8]

ε the inner casing roughness factor, 0.2×10^{-3} m [33]

η_p energy efficiency of injection pump, 80% (our assumption)

ν the kinematic viscosity of geofluid, m^2/s

ρ the geofluid density in wells, kg/m^3

ρ_{ip} geofluid density through injection pump, 977.8 kg/m^3[8]

τ wells operation time, yrs

$\Delta P_{d,iw}$ dynamic pressure change in IW, MPa

ΔP_{ip} geofluid pressure increase in injection pump, MPa

ΔP_{iw} geofluid pressure drop in IW, MPa

ΔP_{pw} geofluid pressure drop in PW, MPa

ΔP_r geofluid pressure drop in reservoir, MPa

ΔT_{iw} geofluid temperature increase in IW, MPa

$\rho_{h,iw}$ density of geofluid in at IW head, kg/m^3

Abbreviations

EES   Engineering Equation Solver

EGS   Enhanced Geothermal System

EROI   energy return on investment

HDR   hot dry rock

IW   injection well

PDC   polycrystalline diamond compact

PW   production well

ROP   rate of penetration

Parameters related to the design guidance for well system (Section 4)

E_{in} energy input to construct the well system, TJ

E_{net} energy output of the EGS well system, TJ

E_{pp} net power output from the surface power plant, MJ

E_{out} net electricity output from the EGS system over its lifetime, TJ

N_{pw} number of PW-s per IW

$P_{b,iw}$ the geofluid pressure at IW bottom, Pa

$P_{b,pw}$ the geofluid pressure at PW bottom, Pa

$P_{h,iw}$ the geofluid pressure at IW head, Pa

$P_{h,pw}$ the geofluid pressure at PW head, Pa

$T_{b,iw}$ the geofluid temperature at IW bottom, °C

$T_{b,pw}$ the geofluid temperature at PW bottom, °C

$T_{h,iw}$ the geofluid temperature at IW head, °C

$T_{h,pw}$ the geofluid temperature at PW head, °C

$(\Delta E_{net})_R$ relative increased net energy output, %

References

[1] Tester JW, Anderson B, Batchelor A, Blackwell D, DiPippo R, Drake E, et al. The future of geothermal energy: impact of enhanced geothermal systems (EGS) on the United States in the 21st century, vol. 209. Massachusetts Institute of Technology; 2006.

[2] DiPippo R. Geothermal power plants: principles, applications and case studies. Oxford; New York: Elsevier; 2005.

[3] Li M, Lior N. Analysis of hydraulic fracturing and reservoir performance in enhanced geothermal systems. J Energy Resour Technol 2015;137:042904.

[4] Augustine C, Tester JW, Anderson B, Petty S, Livesay B. A comparison of geothermal with oil and gas well drilling costs. In: Thirty-first workshop on geothermal reservoir engineering. New York, New York: Curran Associates Inc; 2006. p. 5–19.

[5] Mansure AJ, Bauer SJ, Livesay BJ. Geothermal well cost analyses, vol. 29; 2005. p. 515–9.

[6] Augustine CR. Hydrothermal spallation drilling and advanced energy conversion technologies for engineered geothermal systems. PhD Thesis. Cambridge, MA: MIT; 2009.

[7] Kruger P, Otte C, American Nuclear Society. Geothermal energy; resources, production, stimulation. Stanford, Calif: Stanford University Press; 1973.

[8] Li M, Lior N. Comparative analysis of power plant options for enhanced geothermal systems (EGS). Energies 2014;7:8427–45.

[9] Teodoriu C, Cheuffa C. A comprehensive review of past and present drilling methods with application to deep geothermal environment. In: Thirty-Sixth Workshop on Geothermal Reservoir Engineering, SGP-TR-191. Stanford, California: Stanford University; 2011.

[10] Graves RM, O'Brien DG. StarWars laser technology applied to drilling and completing gas wells. In: SPE Annual Technical Conference and Exhibition. Society of Petroleum Engineers; 1998.

[11] Polsky Y, Capuano Jr L, Finger J, Huh M, Knudsen S, Chip A, et al. Enhanced geothermal systems (EGS) well construction technology evaluation report. SAND2008–7866. Sandia National Laboratories; 2008.

[12] Pessier R, Damschen M. Hybrid bits offer distinct advantages in selected roller-cone and PDC-bit applications. SPE Drill Complet 2011;26:96–103.

[13] Schlumberger. Oil field glossary, http://www.glossary.oilfield.slb.com/en/Terms/l/liner.aspx.

[14] The Physics Hypertextbook. Chemical potential energy. http://physics.info/energy-chemical/.

[15] Edwards LM, Chilingar G, Rieke III H, Fertl W. Handbook of geothermal energy. Houston, TX: Gulf Publishing Company; 1982.

[16] Hammond G, Jones C, Lowrie F, Tse P. Embodied carbon: the inventory of carbon and energy (ICE). BSRIA 2011;201.

[17] American Petroleum Institute. API 5CT specification for casing and tubing. 9th ed. 2011.

[18] Engineering toolbox. Densities of some common materials. http://www.engineeringtoolbox.com/density-materials-d_1652.html.

[19] Mansure A. Engineered geothermal systems energy return on energy investment. No. DOE/EE/0002740-F. 2012.

[20] Engineering Toolbox. Thermal conductivity of some common materials and gases. http://www.engineeringtoolbox.com/thermal-conductivity-d_429.html.

[21] Engineering Toolbox. Densities of miscellaneous solid. http://www.engineeringtoolbox.com/density-solids-d_1265.html.

[22] Dong T. Thermodynamic analysis of thermal responses in horizontal wellbores. J Energy Resour Technol 2015;137:032903.

[23] Zeng Y, Wu N, Su Z, Hu J. Numerical simulation of electricity generation potential from fractured granite reservoir through a single horizontal well at Yangbajing geothermal field. Energy 2014;65:472–87.

[24] Zeng Y, Su Z, Wu N. Numerical simulation of heat production potential from hot dry rock by water circulating through two horizontal wells at Desert Peak geothermal field. Energy 2013;56:92–107.

[25] Hasan AR, Kabir CS. Modeling two-phase fluid and heat flows in geothermal wells. J Pet Sci Eng 2010;71:77–86.

[26] Hasan AR, Kabir CS, Wang X. A robust steady-state model for flowing-fluid temperature in complex wells. SPE Prod Operat 2009;24:269–76.

[27] Hasan AR, Kabir CS, Sarica C. Fluid flow and heat transfer in wellbores. Society of Petroleum Engineers; 2002.

[28] Bejan A, Tsatsaronis G, Moran MJ. Thermal design and optimization. New York: John Wiley; 1996.

[29] Brill J. Multiphase flow in wells. J Pet Technol 1987;39:15–21.

[30] Chen NH. An explicit equation for friction factor in pipe. Ind Eng Chem Fundam 1979;18:296–7.

[31] Mozaffari S, Ehsani M, Nikookar M, Sahranavard L. Heat and mass transfer modeling in wellbore during steam injection process. Can J Chem Eng Technol 2011;2:74–104.

[32] Bergman TL, Incropera FP, Lavine AS. Fundamentals of heat and mass transfer. John Wiley & Sons; 2011.

[33] Çengel YA, Ghajar AJ. Heat and mass transfer: fundamentals & applications. 4th ed. New York: McGraw-Hill; 2011.

[34] Hassan A, Kabir C. Aspect of heat transfer during twophase flow in wellbores. SPE Paper. 1994. p. 211–6.

[35] Pruess K. Enhanced geothermal systems (EGS) using CO2 as working fluid—a novel approach for generating renewable energy with simultaneous sequestration of carbon. Geothermics 2006;35:351–67.

[36] Klein S, Alvarado F. Engineering equation solver. Madison, WI: F-Chart Software; 2002.

[37] Huang X, Zhu J, Niu C, Li J, Hu X, Jin X. Heat extraction and power production forecast of a prospective Enhanced Geothermal System site in Songliao Basin, China. Energy 2014;75:360–70.

[38] Aunzo ZP. Wellbore models GWELL, GWNACL, and HOLA user's guide. Lawrence Berkeley National Laboratory; 2008.

[39] U.S. Energy Information Administration. Electric power monthly with data for March 2015. 2015.

[40] Engineering Toolbox. Critical points some common substances. http://www.engineeringtoolbox.com/critical-point-d_997.html.